Atmospheric Research 315 (2025) 107865

Contents lists available at ScienceDirect

Atmospheric Research

journal homepage: www.elsevier.com/locate/atmosres

Impact of initial intensity error on simulated tropical cyclone track over the western North Pacific

Kyoungmin Kim [a], Woojin Cho [a], Dong-Hyun Cha [a,*], Jinyoung Park [b], Yuqing Wang [c], Johnny C.L. Chan [d]

[a] Department of Civil, Urban, Earth, and Environmental Engineering, Ulsan National Institute of Science and Technology, Ulsan, South Korea
[b] Korea Institute of Science and Technology Information, Daejeon, South Korea
[c] Department of Atmospheric Sciences and International Pacific Research Center, University of Hawaii at Manoa, Honolulu, USA
[d] School of Energy and Environment, City University of Hong Kong, Hong Kong, China

ARTICLE INFO

Keywords:
Tropical cyclone
Numerical weather simulation
Dynamical initialization
Potential vorticity tendency

ABSTRACT

In numerical modeling, uncertainties in the initial intensity of tropical cyclones (TCs) can lead to track errors. In this study, we analyzed the impact of initial intensity error on the simulated TC tracks based on 1128 simulations using the Weather Research and Forecasting (WRF) model for TCs in the western North Pacific between June and November from 2006 to 2018. Results show that the initial TC intensities were largely underestimated compared to observations. In TC cases with the initial intensity error below -10 m s^{-1}, the simulated track position errors (TPEs) were notably greater than TCs in other cases with smaller absolute initial intensity errors. To quantify the positive impact of the improved initial TC intensity on the track simulations, we conducted additional simulations with the dynamical initialization (DI) scheme to enhance the initial TC intensity. Compared to the simulations without the DI scheme, the simulations with the DI scheme performed better in simulating TC tracks, with a 20.3 % reduction in TPE at 72-h. The improvement was understood based on the potential vorticity tendency diagnostic analysis. Results show that the TC motion in the simulations with the DI scheme was controlled by both horizontal and vertical advections, while that without the DI scheme was dominated by horizontal advection only, especially in the early stage of simulations when the TC intensity was considerably underpredicted. The finding highlights the importance of improving the initial TC intensity to the TC track simulations/predictions.

1. Introduction

Tropical cyclones (TCs) are severe weather systems characterized by powerful winds and heavy rainfall, often resulting in significant human and economic damage. Thus, accurate prediction of the track and intensity of TCs is essential to effectively preparing for mitigating the damage caused by TCs. Numerical models are widely used for forecasting the track and intensity of TCs. The performance of numerical modeling for TCs has been improved through advancements in modeling techniques (such as numerical algorithms, physics parameterizations, and model resolution), increased observational data, and computing resources. Nevertheless, there are still factors that may lead to errors when simulating TCs using numerical models. The errors in the TC simulations can be caused by the physics parameterization schemes (Mohan et al., 2019; Park et al., 2023; Zhang and Wang, 2018), model resolution (Gentry and Lackmann, 2010; Ma et al., 2012; Moon et al., 2021a), air-sea interaction (Cho et al., 2022; Zhao and Chan, 2017), and so on.

In the numerical modeling for TCs, uncertainty in the initial condition is another factor that may contribute to errors. Numerical models represent the state of the atmosphere by integrating the governing equations and are sensitive to the initial condition. Even small errors in the initial condition can lead to significant errors in the posterior simulations (Lorenz, 1963). Numerous studies have shown that the initial condition contributes to the accuracy of the TC simulations (Miyachi and Enomoto, 2021; Mohanty et al., 2010; Yamaguchi et al., 2012). Furthermore, the simulated track of TC varies depending on the initial conditions of the TC state (Cao et al., 2011; Fiorino and Elsberry, 1989;

* Corresponding author at: Department of Civil, Urban, Earth, and Environmental Engineering, Ulsan National Institute of Science and Technology, 50 UNIST-gil, Ulju-gun, Ulsan 689-798, South Korea.
E-mail address: dhcha@unist.ac.kr (D.-H. Cha).

https://doi.org/10.1016/j.atmosres.2024.107865
Received 15 July 2024; Received in revised form 6 December 2024; Accepted 6 December 2024
Available online 9 December 2024

Wang et al., 2017). Cao et al. (2011) explored the influence of the initial vortex structure by modifying the size and shape of the wind profile in the initial condition. They demonstrated that the initial core size and outer-core wind structure influenced the speed and landfall time of TCs. Also, Wang et al. (2017) investigated the impacts of initial TC intensity and size on the TC track for Typhoon Megi (2010) using a numerical model. They found that the stronger initial intensity and larger size led the typhoon to turn northward earlier. Since the simulated TC motion is sensitive to the initial TC condition, it is crucial to include realistic information about the TC at the initial condition.

To get a realistic initial condition for a TC, data assimilation (DA) techniques, such as Kalman filters and variational methods, were used. With increasing the observation data, there has been much progress in numerical modeling with TC vortex initialized using the DA technique (Choi et al., 2017; Schwartz et al., 2013; Zhang and Pu, 2019). Nonetheless, observation-based DA techniques are limited by the difficulty of fully observing TCs in space and time. As a different approach to the observation-based DA initialization method, there is another initialization method that uses a bogus vortex created through an empirical function considering the radial profile of the surface pressure and wind. Many studies have shown that TC simulations can be improved by using the bogus vortex as the TC vortex of the initial condition or as the observation for the DA (Kwon and Cheong, 2010; Thu and Krishnamurti, 1992; Wang et al., 2008; Xiao et al., 2009; Zhang et al., 2007). However, the bogus vortex can be physically and dynamically inconsistent with the numerical model. Another initialization method, dynamical initialization (DI), overcomes the weakness of the bogus vortex. The DI has the advantage of being consistent with numerical models because it enhances the TC vortex with an axisymmetric component created by the model integration. The simulations using the DI scheme resulted in better initialized TC vortex and improved TC simulations (Cha and Wang, 2013; Liu and Tan, 2016; Liu et al., 2018). It is considered appropriate to use the DI scheme to obtain improved and model-consistent initial conditions for TC simulations/predictions.

The TC motion is determined by internal and external dynamical processes. George and Gray (1976) demonstrated that there is a strong correlation between the TC motion and its surrounding winds, especially at 500 and 700 hPa. Chan and Gray (1982) also found that the TC motion was consistent with the flow averaged in mid-level horizontal winds between 5 and 7° from the TC center. Furthermore, the large-scale surrounding flow, referred to as steering flow, has been used to understand the TC motion, considering the steering flow depth and the radius of the TC (Ashcroft et al., 2021; Chan, 1985; Torn et al., 2018; Wu and Chen, 2016). In addition, the TC motion is influenced by the vertical structure of the vortex, wind shear, and diabatic heating (Wang and Holland, 1996; Wang, 1998; Yamada et al., 2016). For example, Yamada et al. (2016) investigated the role of vertical structure in the simulated northward bias for Typhoon Fengshen in 2008. In their simulations, weak vertical interactions caused the tilt of the vortex, and the northward bias was driven by northward wind at low levels. As mentioned in the previous studies, the TC motion is driven by a variety of dynamical and physical processes, and those processes need to be considered together to better understand the TC motion. The use of a potential vorticity tendency (PVT) framework is effective in understanding the physical mechanisms of the TC motion. The PVT framework was proposed by Wu and Wang (2000) as a method to diagnose TC motion through the asymmetric structure of the PVT. The solution of the PVT equation can represent TC motion by taking into account steering flow, vertical structure, and diabatic heating. Therefore, we adopted the PVT framework to understand the TC motion of the simulated TCs in this study.

The purpose of this study is to investigate the impact of the initial TC intensity errors on the TC track simulations. The TC simulations were performed for the TCs in the western North Pacific (WNP), and the relationship between the initial TC intensity error and TC track error was analyzed. The performance of the TC track simulations with the improved initial intensity was verified by evaluating the experiments where the initial TC intensity was improved by the DI scheme. The PVT framework was also used to analyze the changes in the physical mechanisms related to the TC motion with the initial intensity. The remainder of the article is organized as follows. The methodologies and modeling approach are described in section 2. The performance of the TC track simulations is presented in section 3. The PVT diagnosis results are discussed in section 4. The summary and discussion are given in section 5.

2. Methodologies and modeling approach

2.1. Model Setup and experimental design

The numerical model used in this study was the Weather Research and Forecasting (WRF) model, version 3.7.1 (Skamarock et al., 2008) (Supplementary Table S1). The domain of the WRF model was set as a single domain with a grid resolution of 12 km. The single domain consists of 421 grid points in the x-direction and 371 in the y-direction. The center of the domain was set for each TC due to the computational resource limitations. Thus, we set the center of the domain based on the latitude in two ways: the center of the domain was positioned 10° northwest of the typhoon center if the initial TC position was south of 20°N, the center of the domain was positioned 10° north of the TC center for the cases in which the initial TC position was north of 20°N. There are 35 vertical layers with 50 hPa as the pressure at the model top. Physics options in the model were the WRF single-moment 6-class microphysics scheme (Hong and Lim, 2006), rapid radiative transfer model long-wave radiation scheme (Mlawer et al., 1997), Dudhia shortwave radiation scheme (Dudhia, 1989), Kain-Fritsch cumulus parameterization scheme (Kain, 2004), Yonsei University planetary boundary layer scheme (Hong et al., 2006). The TC simulations with the WRF model were conducted for 72-h.

To investigate the impact of the improved initial TC intensity on the TC track simulations, we additionally simulated TCs by adjusting the initial intensity to be similar to that from Regional Specialized Meteorological Centers (RSMC) best track data. In this study, we employed the DI scheme proposed by Cha and Wang (2013). The DI scheme consists of model integration, vortex separation, and performing cycle runs for TC vortex spin-up and relocation. The DI scheme can enhance only the vortex component of the TC while keeping the environmental field as unchanged as possible. For further details, we refer to Appendix A, which provides a detailed explanation based on Cha and Wang (2013).

The domain setting of the DI experiments in this study differs from that of Cha and Wang (2013). In the DI scheme, high-resolution simulations are required to simulate TCs realistically. The nested domain was added to the WRF model configuration only for the cycle runs of the DI scheme in this study. The grid of the nested domain had a horizontal resolution of 4 km, with dimensions of 514 × 514. The model simulations were conducted in the nested domain with the cumulus scheme turned off. In addition, the enhanced vortex by the DI scheme should be located at the initial TC position in the WRF model to exclude the effect of the initial position error on the TC track simulations. After the cycle run, we relocated the vortex to the initial position of the TC in the WRF model and ran for 72-h with the single domain. Moreover, spectral nudging (von Storch et al., 2000) was applied for 6-h from the initial time after the final cycle run of the DI process to ensure model stabilization. In this study, we compared the experiments without the use (hereafter referred to as the CTL run) and with the use of the DI scheme (hereafter referred to as the DI run) to investigate the effect of initial intensity errors on the simulated track errors.

To analyze the impact of the initial TC intensity error on the performance of the simulated TC tracks, all experiments were executed with the NCEP Final (FNL) Operational Global Analysis data 1° × 1° as the initial and lateral boundary conditions, except for the initial condition of the DI runs where the initial TC vortex was dynamically initialized. The

results of all experiments were validated using the RSMC best track data. Moreover, we selected TC cases occurring in the WNP from June to November between 2006 and 2018 and conducted a total of 1128 simulations for 182 TC cases (Supplementary Table S2). Also, we only conducted the simulations for the periods when the TC maintained the intensity of tropical storms (defined as 17 m s^{-1}) or stronger.

2.2. Potential vorticity tendency diagnostic framework

We utilized the PVT diagnostic framework to understand the motion of the simulated TCs. The PVT diagnostic method helps to understand the physical mechanisms of TC motion (Wu and Wang, 2000). The motion of TCs has the tendency to move toward the maximum of PVT wavenumber (WN) 1. The TC motion is related to PVT WN1, as described in Eq. (1):

$$-C_x\left(\frac{\partial P_s}{\partial x}\right)_i - C_y\left(\frac{\partial P_s}{\partial y}\right)_i = \left(\frac{\partial P}{\partial t}\right)_{1i} \quad (1)$$

where P represents the potential vorticity; P_s is the symmetric components of potential vorticity; C_x and C_y are the zonal and meridional components of the TC motion; the right term of Eq. (1) is the wavenumber 1 component of the PVT framework.

The PVT equation was defined as follows:

$$\left(\frac{\partial P}{\partial t}\right)_1 = \wedge_1\left\{-u\frac{\partial P}{\partial x} - v\frac{\partial P}{\partial y} - \dot{\sigma}\frac{\partial P}{\partial \sigma} + \frac{g}{p_s}\left[-\{\xi+f\}\frac{\partial \dot{\theta}}{\partial \sigma} - \frac{\partial u}{\partial \sigma}\frac{\partial \dot{\theta}}{\partial y} + \frac{\partial v}{\partial \sigma}\frac{\partial \dot{\theta}}{\partial x}\right]\right\} \quad (2)$$

where $\wedge_1$ is the operator to obtain the wavenumber 1 component; g is the gravitational acceleration; p_s is the surface pressure; ξ and f are the relative vorticity and the Coriolis parameter, respectively; u and v are the zonal and meridional wind components; θ is the potential temperature; $\dot{\sigma}$ is the vertical velocity in the σ coordinate. Furthermore, Eq. (2) can be divided into horizontal advection (HA), vertical advection (VA), and diabatic heating (DH): HA is $-u\frac{\partial P}{\partial x} - v\frac{\partial P}{\partial y}$; VA is $-\dot{\sigma}\frac{\partial P}{\partial \sigma}$; DH is $\frac{g}{p_s}\left[-\{\xi+f\}\frac{\partial \dot{\theta}}{\partial \sigma} - \frac{\partial u}{\partial \sigma}\frac{\partial \dot{\theta}}{\partial y} + \frac{\partial v}{\partial \sigma}\frac{\partial \dot{\theta}}{\partial x}\right]$. Wu and Wang (2000) also suggested that the impact of various physical processes on the PVT WN1 can be calculated, allowing for the analysis of contributions of HA, VA, and DH to the TC motion. The dominant component determines the tendency of the TC motion, and thus the most influential physical processes from PVT can be identified. Moon and Ha (2019) determined the analysis targets, such as asymmetric flow and a vertical structure, by considering the tendency for each component in the PVT for their TC simulations. Hsu et al. (2021) showed that the VA and DH components of the PVT significantly influenced the track of Typhoon Saola near the northeast of Taiwan in 2012.

In this study, we applied the PVT diagnostic framework for the CTL and DI runs and examined the dominant components to analyze the processes influencing the TC motion. The maximum point of PVT WN1 was generally located within 50 km of the maximum potential vorticity in each vertical layer (not shown). Accordingly, we specified a square domain (100 km × 100 km) centered on the point of maximum potential vorticity and measured C_x and C_y of PVT within this domain using the least squares method. In addition, each TC has a different vertical layer of PVT associated with the TC motion (Chan et al., 2002; Choi et al., 2013; Xie et al., 2022). We investigated the vertical layers of PVT, from lower to upper levels (0.9–0.25 sigma level; 900–300 hPa), highly correlated with the simulated TC motion for each simulation. The optimal vertical layer was determined based on the similarity in direction of the simulated TC motion to diagnose the TC motion through the PVT framework. A total of 105 vertical layer sets were investigated with vertical layers at 0.05 interval between 0.9 and 0.25 sigma level. Furthermore, the dominant component among the PVT WN1 components was selected based on the magnitude and direction of the motion vectors in each component, considering the TC motion vector of PVT. The TC motion vector of the simulation was calculated as the difference between the current position and the position 12-h later.

3. Results and discussions

3.1. The performance of the TC track simulation

We evaluated the uncertainty in the initial condition of the TCs based on the TC intensity. The TC intensity was defined as the maximum surface wind speed (MWS) near the center of the TCs. In this study, we compared the MWS from the initial conditions in FNL for the 1128 simulations to that of the RSMC best track (Fig. 1). In most cases, the MWS of the FNL initial condition was underestimated compared to that of the RSMC best track. The averaged difference in the MWS between the FNL initial condition and the RSMC best track was −6.1 m s^{-1}. Moreover, the range of the MWS differences increased with an increasing in MWS in the RSMC best track. This implied that for the cases selected in this study, most initial conditions were in a state of weak TC intensity compared to the observations. In particular, the real stronger TCs were underrepresented in the initial condition as weaker TCs. This underestimation in TC intensity is a general characteristic of other global models (Hodges and Klingaman, 2019; Majumdar et al., 2023).

The performance of the WRF model in simulating TC tracks was analyzed by calculating the track position error (TPE) from the RSMC best track. TPE was defined as the great circle distance between the center of the best track data and the center of the simulated TC. TPE was calculated using the Haversine formula (Neumann and Pelissier, 1981; Powell and Aberson, 2001):

$$TPE = 111.11cos^{-1}[sin\varphi_0 sin\varphi_s + cos\varphi_0 cos\varphi_s cos(\lambda_0 - \lambda_s)] \quad (3)$$

where λ_s and φ_s are the longitude and latitude of the simulated TC position and λ_0 and φ_0 are the longitude and latitude of the TC position from the best track, respectively. Fig. 2 shows the TPE of the simulated 72-h TC tracks at 6-h intervals for 1128 simulations. The median of TPEs at 24-h, 48-h, and 72-h are approximately 66.7 km, 110 km, and 172 km, respectively. The TPEs of those simulations increased linearly with the forecast lead time. In addition, at 72-h, the TPE was up to 1290.4 km. With the increasing TPE trend, the spread of TPE dramatically increased

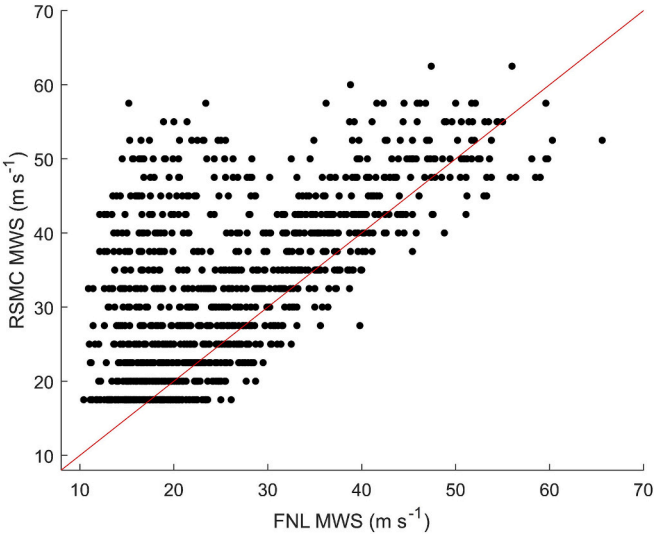

Fig. 1. Scatter plots of TC maximum near-surface wind speed in FNL and RSMC. The red line indicates y = x. (For interpretation of the references to colour in this figure legend, the reader is referred to the web version of this article.)

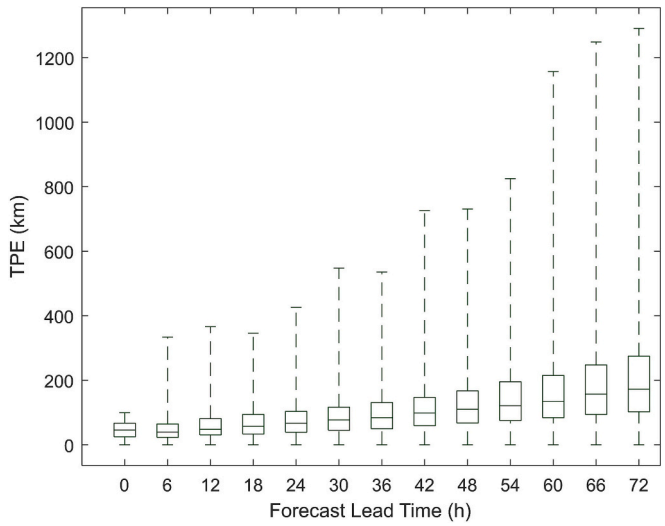

Fig. 2. Box plots of TPEs for the 1128 TC simulations. The box indicates the 25th and 75th percentiles of the error distribution, and the line in the box indicates the median. The top and bottom lines connected to the box indicate the maximum and minimum values, respectively.

as the forecast lead time increased. The tendency of this TPE in numerical models for TCs is expected as shown in other studies (Chen et al., 2021; Lui et al., 2021; Moon et al., 2021b). The initial TC intensity errors and TPEs shown in Figs. 1 and 2 are reasonable. To understand the relationship between the initial TC intensity error and the TPE, it is necessary to perform a detailed analysis based on the initial TC intensity.

To analyze the effect of initial intensity errors on the track simulations, all simulations were classified into nine categories according to the initial MWS errors: C1 (<-30 m s^{-1}), C2 (-30 to -25 m s^{-1}), C3 (-25 to -20 m s^{-1}), C4(-20 to -15 m s^{-1}), C5(-15 to -10 m s^{-1}), C6 (-10 to -5 m s^{-1}), C7(-5 to 0 m s^{-1}), C8(0 to 5 m s^{-1}), C9(>5 m s^{-1}). The number of simulation cases for C1 to C9 was 26, 38, 54, 57, 89, 223, 344, 239, and 58, respectively. We evaluated the averaged TPE for each category by the forecast lead time with the averaged TPE of all simulations. Fig. 3 shows the averaged TPEs at 24-h (red), 48-h (blue), and

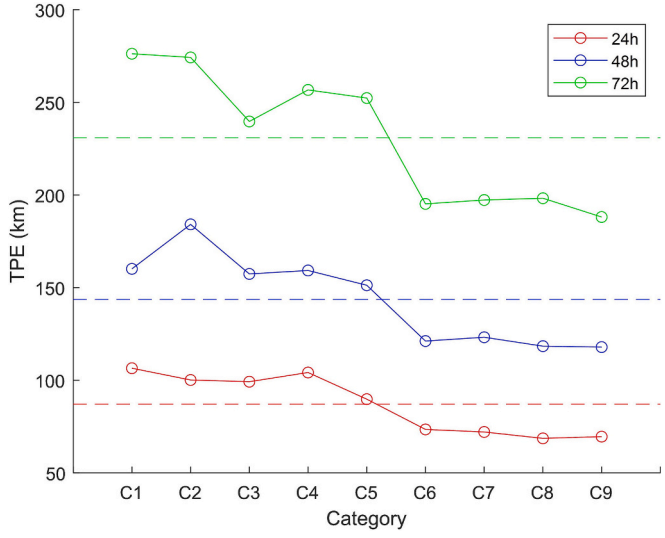

Fig. 3. Averaged TPEs for each category (solid line) and averaged TPEs for TPE_{ALL} (dash line) in each forecast lead time. The red, blue, and green lines indicate TPEs for 24-h, 48-h, and 72-h, respectively. (For interpretation of the references to colour in this figure legend, the reader is referred to the web version of this article.)

72-h (green) lead-time forecasts according to the initial MWS error for each category. In the analysis of averaged TPEs based on the forecast lead time, the largest TPEs were 106 km for C1 at 24-h, 184 km for C2 at 48-h, and 276 km for C1 at 72-h, respectively. C1 to C5 had larger averaged TPEs than that of all simulations, while no category from C6 to C9 had averaged TPEs that exceeded the averaged TPE of all simulations for each forecast lead time. Based on the averaged TPE of all simulations, the difference in averaged TPEs between the larger TPE groups (C1 to C5) and smaller TPE groups (C6 to C9) increased with the forecast lead time. This indicates that the more the underestimation of the initial TC intensity, the larger the TPE. In addition, the cases with initial MWS errors below -10 m s^{-1} exhibited a rapid increase in TPE with increasing forecast lead time compared to the other cases. Consequently, the underestimated initial TC intensity contributed to the worse performance of the TC track simulations. Since the TC tracks are simulated differently depending on the TC intensity (Cao et al., 2011; Fiorino and Elsberry, 1989; Wang et al., 2017), the initial condition with underestimated TC intensity may lead to different simulated TC tracks from the observations.

The impact of the initial TC intensity errors on the TC track simulations was analyzed in detail by improving the initial TC intensity. The initial TC intensity was improved by applying the DI scheme described in section 2, which has the advantages such as increasing the TC intensity without changing the surrounding environment and the consistency of the model dynamics and physics (Cha and Wang, 2013). The cases selected for applying the DI scheme were based on the initial TC intensity error and the TPE. As shown in Fig. 3, the cases with the initial MWS error below -10 m s^{-1} performed poorly in the TC track simulations, with the averaged TPEs of more than 230.87 km, which is the averaged TPE for all simulations at 72-h. Therefore, for C1 to C5, the DI scheme was applied to the cases where the TPE at 72-h exceeded 230.87 km. We also excluded the cases where the terrain was located within the TC radius estimated by the DI scheme. Because the TC structure can be distorted by topographic effects when the vortex relocation of the DI scheme is performed (Hsiao et al., 2010). Consequently, we compared the CTL runs and the DI runs for 51 cases (Supplementary Table S3).

The initial intensity of the 51 selected cases was successfully improved through the application of the DI scheme. The averaged MWS error for DI runs was -3.35 m s^{-1}, which is smaller than the averaged MWS error of -21.47 m s^{-1} for CTL runs (Table 1). The initial intensities of the DI runs were very similar to observations compared to the initial intensities of the CTL runs. The application of the DI scheme resulted in an enhanced initial TC intensity closer to the RSMC best track. In addition, since the DI scheme only changes the environment within the TC radius, we were able to focus on the effects of TC intensity changes. To support the intensification of only TC scales, we took Typhoon Shanshan at 0000 UTC 13 September 2006 as an example to compare the intensity of each cycle run with the TC state (Fig. 4). The MWS of the RSMC best track at 0000 UTC 13 September 2006 was 42.5 m s^{-1}. However, the MWS in FNL as the initial condition of WRF was 11.82 m s^{-1}, which was significantly weaker than that in the RSMC best track (Fig. 4g). To obtain the MWS similar to the RSMC best track, we conducted 15 cycle runs using the DI scheme. As the number of cycle runs increased, the MWS of the initial condition increased toward that close to the MWS of the RSMC best track. After the final cycle run, the MWS became 44.71 m s^{-1}, which was much stronger compared to the FNL. This indicates that the MWS of the initial condition was successfully

Table 1
TC intensity errors averaged at the initial time for the 51 simulations. Intensity error is calculated for the maximum near-surface wind speed.

Expt.	MWS error (m s^{-1})
CTL	−21.47
DI	−3.35

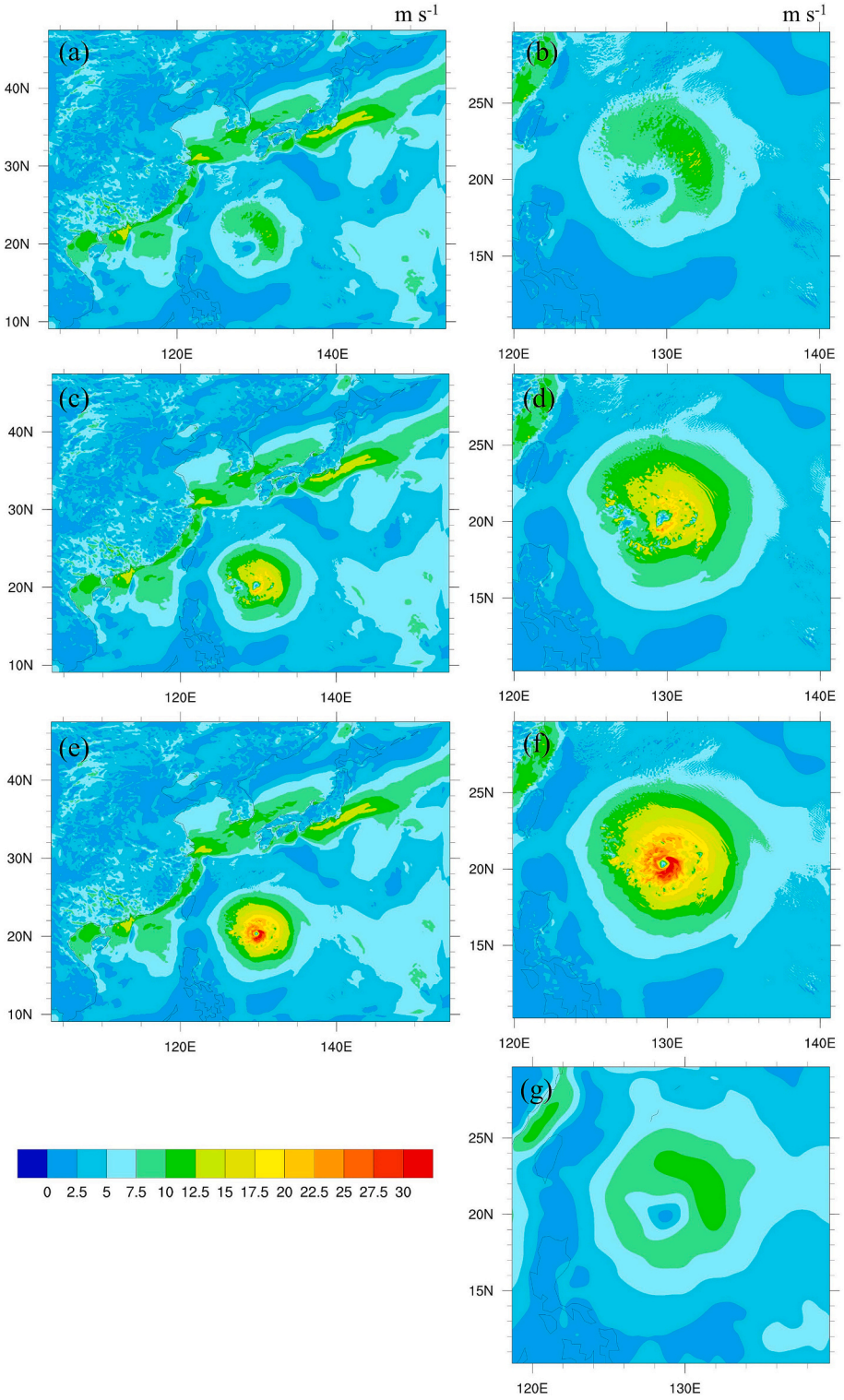

Fig. 4. Near-surface wind speed (m s^{-1}) for Typhoon SHANSHAN at 0000 UTC 13 Sept. 2006 in domain 1 (left) and domain 2 (right) from cycle 1 (a, b), cycle 9 (c, d), cycle 15 (e, f) and FNL (g).

strengthened through the DI scheme for Typhoon Shanshan. Moreover, it is notable that there was little change in the environment around the TC as it intensified. When comparing domain 1 (Figs. 4a, c, e) and domain 2 (Figs. 4b, d, f) of each cycle run, the surface wind increased in the vicinity of the TC located at 20.3°N and 129.8°E. However, there was little or no change in wind speed outside a distance of about 690 km from the center of the TC. The results of the DI application indicated that the DI scheme was appropriate for analyzing the impact of enhanced initial TC intensity on the TC track simulation without changing the environmental field.

Fig. 5 shows the averaged TPEs of the CTL and DI runs for the TC track simulation over 72-h. The averaged TPEs at the initial time were 42.3 km for the CTL runs and 44.1 km for the DI runs, respectively. Because the vortex enhanced by the DI scheme was relocated to the

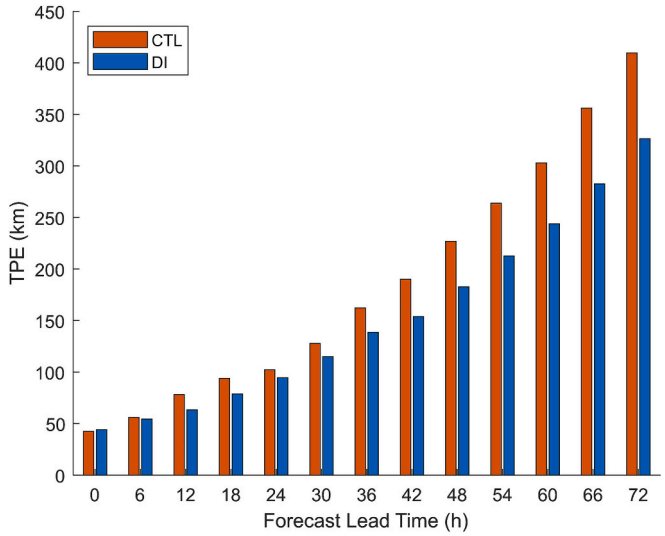

Fig. 5. Averaged TPEs for the 51 simulations of the CTL runs, and the DI runs.

initial position of TCs in the CTL runs, the CTL and DI runs had similar averaged TPE at the initial time. Compared to the RSMC best track, the DI run had a smaller initial MWS error than the CTL run, as shown in Table 1. This means that the CTL and DI runs had a similar TC position in the initial conditions, but the DI runs started from a TC state with an intensity similar to that of the observations compared to the CTL runs. Comparing the performance of the TC track simulations, the averaged TPEs of DI runs were smaller than CTL runs at all forecast lead times after the initial time. The TPEs of the DI runs were slightly smaller than those of the CTL runs in the early stages of the simulations. After 30-h, the TPE of the CTL runs increased rapidly compared to that of the DI runs, with the TPEs at 72-h being 409.7 km for the CTL runs and 326.4 km for the DI runs, respectively. There was a 20.3 % improvement in the TC track simulations at 72-h with the DI scheme. The performance of the TC track simulations was improved when the initial TC intensity was made similar to the RSMC best track. To simulate TC tracks accurately, the initial condition with accurate initial TC intensity is required. It was verified through simulations applying the DI scheme that initial TC intensity error affects the TC track simulation. In addition, the application of the DI scheme resulted in dynamic and thermodynamic changes within the TC, such as horizontal wind intensification, deeper TC circulation, and distinct eyewall structure. These changes by the DI scheme can lead to changes in the mechanism of the TC motion. In the next section, we analyzed the changes to the TC motion as the initial TC intensity was enhanced.

3.2. Potential vorticity tendency diagnosis results

The DI runs, where the initial TC intensity was enhanced by applying the DI scheme, performed better than the CTL runs in simulating the TC track, as shown in Fig. 5. We further analyzed the simulated TC track results from the CTL and DI runs for changes in the TC motion due to the improvement of the initial TC intensity. To analyze the impact of the initial condition on TC motion, we employed the PVT framework (Wu and Wang, 2000), which is a good diagnostic tool for analyzing TC motion in terms of its dynamic and thermodynamic impacts on TC motion. In this study, the TC motion of CTL and DI runs were diagnosed using the PVT framework. The diagnostics of the simulated TC motion with the PVT framework were conducted for the earlier part of the simulations to focus on the impact of the initial condition on TC motion. We analyzed the simulated TC motion for 12-h from 6 to 18-h of the simulations because spectral nudging was used for the model stabilization from the initial time to 6-h after the final cycle run of the DI process.

In addition, for the PVT diagnosis, each TC case had different vertical layers directly related to the simulated TC motion, as mentioned in section 2.2. Therefore, we optimized the vertical layers to be used within the PVT diagnosis based on the direction of the simulated TC motion for each simulation case. To evaluate the performance of the TC motion diagnosis using the PVT framework, the diagnosed TC motion vectors (TC_{PVT}) were compared with the simulated TC motion vectors (TC_M) for the early 12-h of the simulation. Table 2 shows the averaged difference between TC_{PVT} and TC_M from 6-h to 18-h for CTL and DI runs. Comparing TC_{PVT} and TC_M in terms of magnitude, the averaged differences were -2.7 m s^{-1} for the CTL runs and -1.2 m s^{-1} for the DI runs. The averaged difference in direction was about 5.3° and 3.6° for CTL and DI runs, respectively. In the PVT diagnosis, the magnitude of TC_{PVT} was underestimated compared to the TC_M in both CTL and DI runs. However, the direction of TC_{PVT} was relatively similar to that of TC_M. Considering the direction, the simulated TC motion can be reasonably diagnosed through the PVT framework.

The advantage of using the PVT framework to diagnose TC motion is that it can identify the dynamic and thermodynamic processes affecting TC motion within the TC scale. The PVT equation can be divided into three components, HA, VA, and DH, according to the order of the horizontal flow, vortex structure, and diabatic heating, as mentioned in section 2.2. The impact of the three components on TC motion can be confirmed by calculating the motion vectors for each component and considering their direction and magnitude when compared to TC_{PVT}. To further explain the impact of HA, VA, and DH on TC motion, we applied the PVT diagnosis for Typhoon Yagi as an example to compare the TC motion of CTL and DI run (Fig. 6). This is one of the examples where the initial TC intensity was successfully improved by the DI scheme, and the performance of the TC track simulation was improved compared with the CTL run (Supplementary Fig. S1). For the TC motion from 6-h to 18-h, both the CTL run and DI run simulated Typhoon Yagi moving westward. Comparing TC_{PVT} to TC_M for the CTL run, the direction of the TC_{PVT} integrated from sigma level 0.82 to 0.69 (near 840 to 710 hPa) was similar to that of TC_M (Fig. 6a). Splitting TC_{PVT} into HA, VA, and DH, the motion vectors of each component were different in terms of magnitude and direction. The magnitude of HA is much larger than those of the other two components. Moreover, the direction of HA was westward, which is similar to the direction of TC_{PVT}, while the directions of VA and DH were northeastward and northwestward. For the DI run, the TC_{PVT} integrated from sigma levels 0.74 to 0.45 (near 760 to 480 hPa) was closest to TC_M for the direction of the motion vector (Fig. 6b). Analyzing HA, VA, and DH for the DI run, HA and VA were similar in magnitude with a westward direction. However, the magnitude of the DH was negligible compared to HA and VA. Consequently, HA had a greater influence than the other components on the simulated westward motion of the TC in the CTL run. In contrast, the TC in the DI run moved westward mainly by the impact of HA as well as VA. In other words, the dominant components determining the motion of the TC in the CTL and DI run were different, even though the TCs moved in the same direction. This is because of the different contributions by VA, which is closely related to the strength of the simulated TC eyewall and thus the TC intensity.

To identify which PVT components are dominant in determining the simulated TC motion, we compared the motion vectors of the PVT components to TC_{PVT}. The impact of each component was quantified using the inner product to simultaneously consider the direction and

Table 2
The averaged difference in TC_{PVT} from TC_M from 6-h to 18-h for 51 CTL and DI runs, separately.

Expt.	Difference ($TC_{PVT} - TC_M$)	
	Direction (°)	Magnitude (m s^{-1})
CTL run	5.3	−2.7
DI run	3.6	−1.2

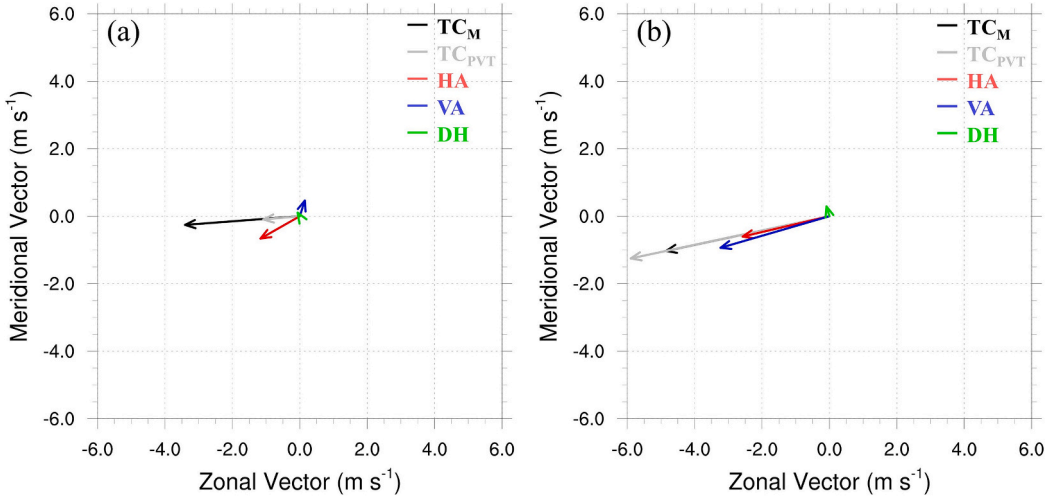

Fig. 6. PVT diagnosis of (a) the CTL run and (b) the DI run during 06 to 18-h forecast lead times for Typhoon Yagi with the initial forecast time at 0000 UTC 19 September 2006. The black arrow indicates TC_M. The other arrows represent the variations of the contributions of TC_{PVT} (gray) by HA (red), VA (blue), and DH (green), respectively. (For interpretation of the references to colour in this figure legend, the reader is referred to the web version of this article.)

magnitude based on TC_{PVT}. The magnitudes of the PVT components' impacts are described in Eq. (4):

$$M_N = \frac{\vec{N} \bullet \overrightarrow{TC_{PVT}}}{\left|\overrightarrow{TC_{PVT}}\right|} \tag{4}$$

where M_N is the magnitude of each PVT component's impact on TC_{PVT}; N is each PVT component. M_N of the PVT component that affects the TC PVT in the same (opposite) direction is positive (negative). Additionally, the absolute value of M_N increases as the impact on TC_{PVT} increases. Fig. 7 shows the magnitude of each PVT component impact for the 51 cases of the CTL and DI runs from 6 to 18-h. Comparing each PVT component for the CTL runs, the median of M_{HA} was 0.85, which was larger than the other components (Fig. 7a). On the other hand, the median of M_{VA} and M_{DH} were close to zero compared to M_{HA}. These results indicated that HA was the most dominant PVT component for the simulated TC motion in the CTL runs. In the early part of the simulation, HA aligned in a direction that was the same as the direction of the simulated TC motion. Compared to HA, the impacts of VA and DH on the simulated TC motion were small, with VA having more impact in the opposite direction of the TC motion. Analyzing the magnitude of each component in TC_{PVT} for the DI runs, the median of M_{HA} and M_{VA} were 1.29 and 1.39, respectively, which had a similar impact on TC_{PVT}. In contrast to the CTL runs, M_{VA} was mostly positive and had a wider distribution than M_{HA}, with a larger magnitude of impact on TC_{PVT}. This means that HA and VA had a positive influence on the direction of the simulated TC motion in the DI runs. Furthermore, VA can have a slightly greater influence on TC motion than HA. DH had a negligible impact on TC_{PVT} in magnitude and direction compared to HA and VA. In summary, HA was the critical component in the CTL runs for the direction of the TC motion, while HA and VA were the dominant components in the DI runs.

The PVT diagnosis confirmed that the difference between the CTL and DI runs was the contribution of VA to the TC motion. The impact of VA on the TC motion was determined by the vertical structure of the TC. To compare the CTL and DI runs for the vertical structure of the TC, the vertical-radial structure of the azimuthal mean vertical velocity, tangential wind, radial wind, and temperature anomaly from 6 to 18-h relative to the TC center are shown in Fig. 8. The temperature anomaly was the temperature difference calculated from the horizontal mean within a 5° radius of the TC center. For the structure of the simulated TCs, the vertical motion of the DI runs was stronger than that of the CTL runs. Furthermore, the tangential and radial winds were significantly stronger in the DI runs than in the CTL runs. When analyzing the radius of 34 knots (~17 m s^{-1}) winds (R34) as the outer size of the TC, the average R34 values for the CTL runs and the DI runs were 299.9 km and 356.4 km, respectively. The simulated TC in the DI runs had a higher height and larger size than in the CTL runs. With this flow around the TC center, the warm core structure was strengthened in the DI runs compared to the CTL runs. For simulations from 6 to 18-h, the structure

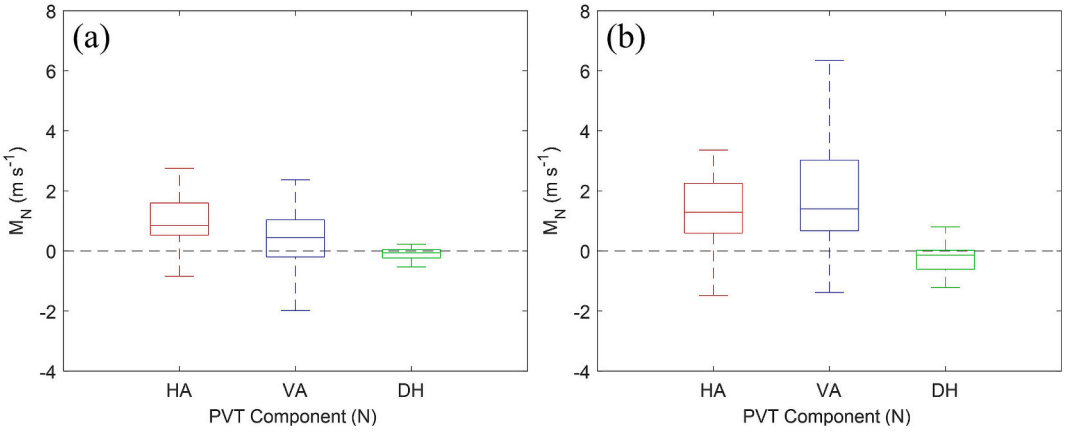

Fig. 7. Boxplots of the magnitude for each PVT component impact on TC_{PVT} at 6–18 h for (a) CTL runs and (b) DI runs.

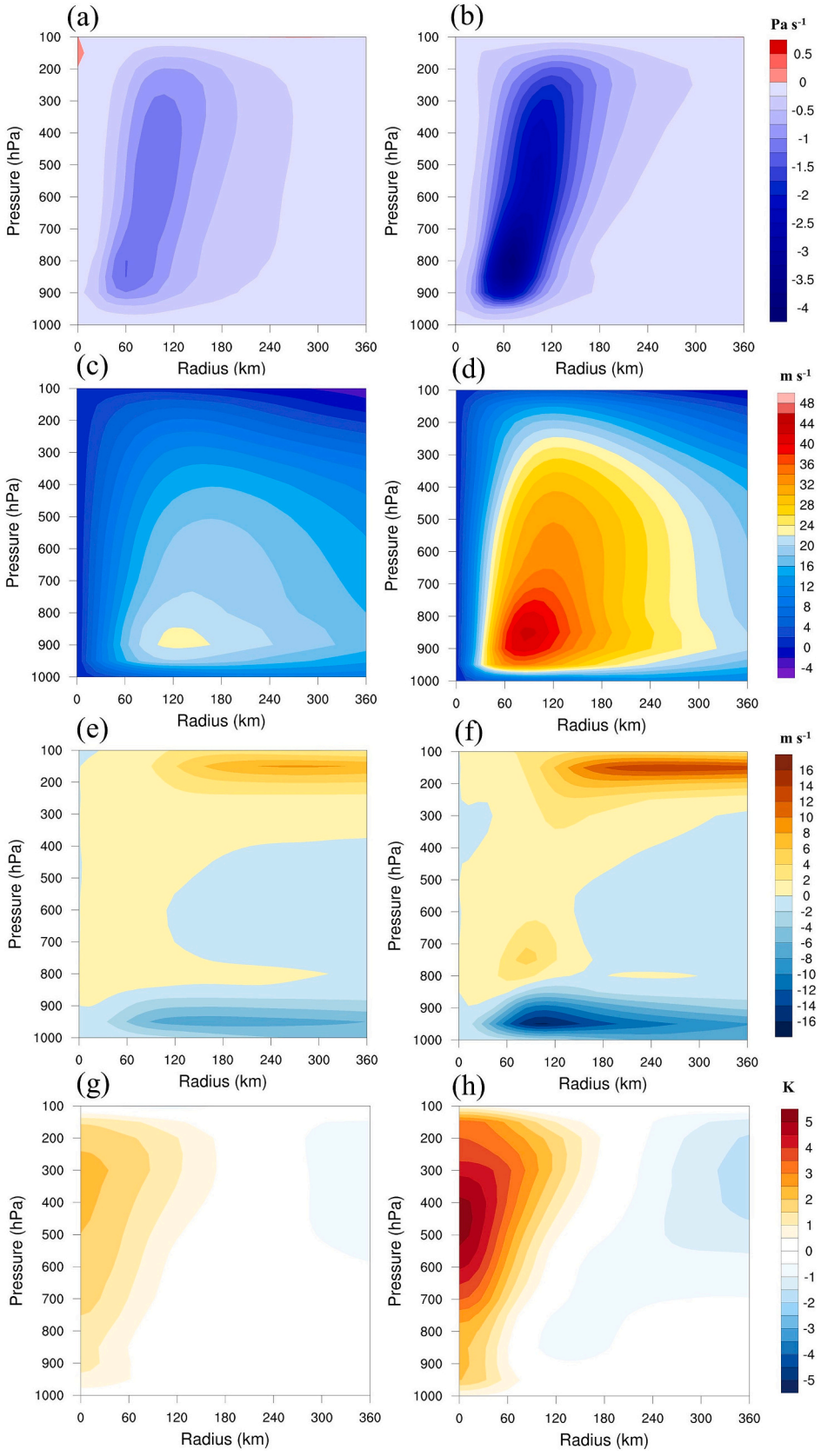

Fig. 8. The azimuthal mean structure of the simulated tropical cyclone averaged for the CTL (Left) and the DI (Right) runs between 06 and 18-h of the simulation: (a) and (b) vertical velocity (Pa s^{-1}), (c) and (d) tangential wind (m s^{-1}), (e) and (f) radial wind (m s^{-1}), (g) and (h) temperature anomaly (K).

of the simulated TC was well developed with the DI scheme compared to that in the CTL runs. Consequently, in the DI runs, there was a stronger updraft around the TC center compared to the CTL runs. Additionally, the radial inflow at the lower levels and the outflow at the upper levels were larger in the DI runs than in the CTL runs. With these primary and secondary circulations, the strong warm cores were exhibited in the DI runs, while the warm cores in the CTL runs were quite weak. The enhanced TC circulations through the DI scheme could lead to the intensification of vertical advection, with a larger contribution of VA to TC motion.

To further analyze the intensification of vertical advection through the DI scheme, the distribution of potential vorticity and the wind field around the TC center were analyzed. Fig. 9 shows the vertical cross-sections through the TC center in the direction parallel to the vertical advection of the PVT diagnosis for the CTL and DI runs. In the CTL runs, the value of potential vorticity was small and widely distributed within a 200 km radius from the TC center (Fig. 9a). However, the DI run had the largest value of potential vorticity at about 750 hPa at the TC center, with higher potential vorticity distributed than that in the CTL runs. In addition, the stronger vertical motion was identified near the TC center compared to the CTL runs similar to Fig. 8b (Fig. 9b). With this distribution feature of potential vorticity, the gradient of potential vorticity in the CTL runs was small, and the variation of potential vorticity in the vertical direction was minimal (Fig. 9c). In the DI runs, the gradient of the potential vorticity was larger than that in the CTL runs, and stronger vertical motion was also identified in areas with large values of vertical potential vorticity gradient (Fig. 9d). Analyzing the number of maximum potential vorticity points used in the PVT diagnosis, the numbers were similar for vertical layers and radii from the TC center for the CTL runs (Fig. 9e). On the other hand, the numbers for the DI runs were higher at about 800 hPa compared to the other vertical layers (Fig. 9f). In addition, the numbers were concentrated within 100 km of the TC center. The PVT diagnoses in the DI runs were performed in regions with larger gradients of potential vorticity or stronger vertical motion compared to those in the CTL runs. Therefore, the impact of vertical advection was considerably greater in the DI runs than in the CTL runs.

4. Summary and discussion

We investigated the impact of the initial TC intensity errors on the TC track simulations over the WNP. We selected TC cases with tropical storm intensity or stronger that occurred in the WNP between June and November from 2006 to 2018. In most cases, the initial TC intensity was

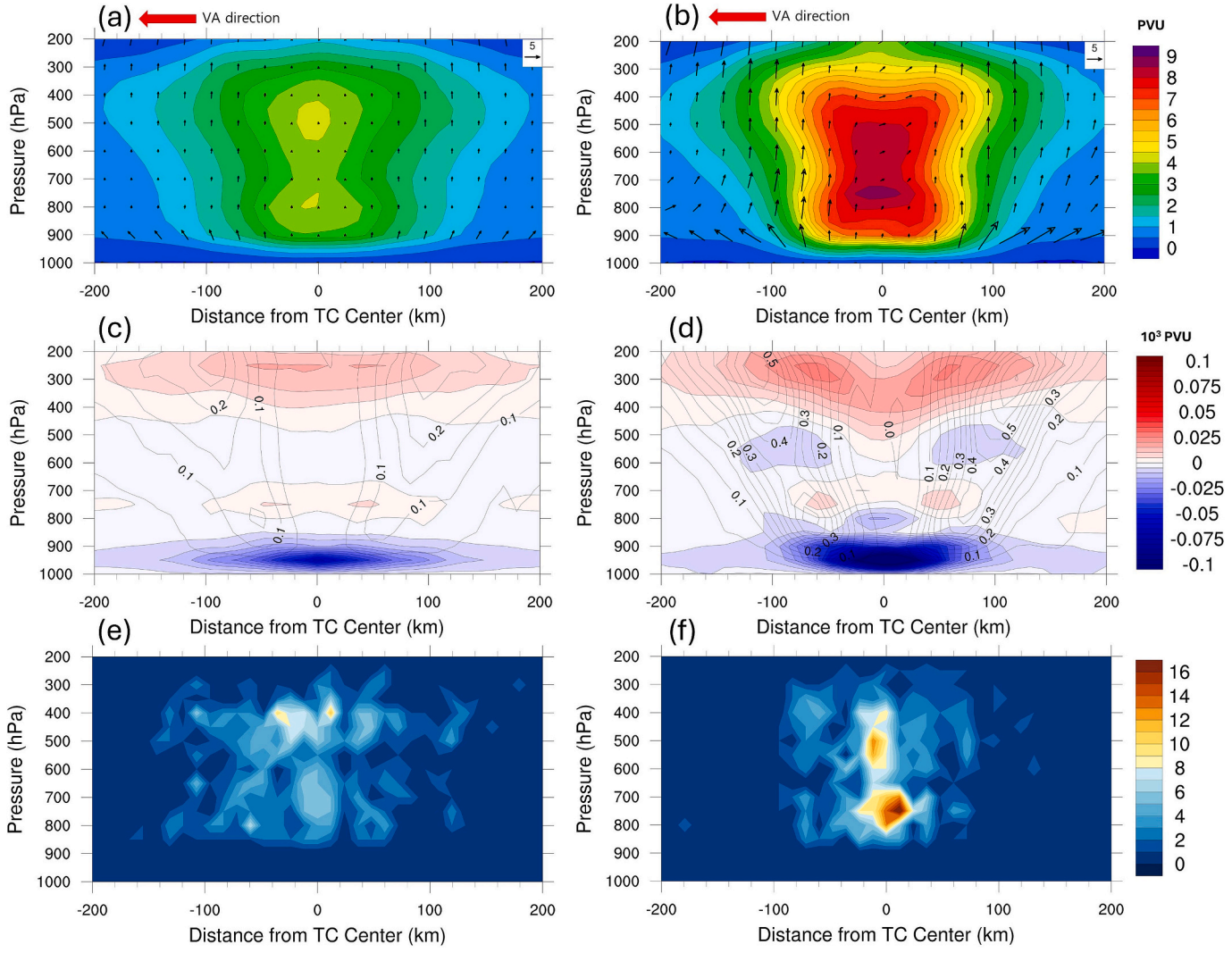

Fig. 9. Vertical cross sections through the TC center in the direction parallel to the vertical advection of the PVT diagnosis for the CTL (left) and DI (right) runs. The top panels show the distribution of potential vorticity (shaded, PVU) and wind fields (Horizontal and W x 10 components, vector, m s^{-1}). The middle panels show the vertical gradient of potential vorticity (shaded, 10^3 PVU) and vertical velocity (contour, m s^{-1}). The bottom panels show the number of maximum potential vorticity points used in the PVT diagnosis.

underestimated compared to the RSMC best track by a mean bias of -6.1 m s^{-1}. With the initial conditions containing underestimated TC intensity, the averaged TPEs of the TC simulations ranged from 66.7 km at 24-h to 172 km at 72-h. To investigate the impact of the initial TC intensity error on the performance of the TC track simulations, we classified the TC simulation results into nine categories based on the initial TC intensity errors. The results showed that the cases with the initial MWS errors below -10 m s^{-1} had higher averaged TPEs than the averaged TPE for all simulations at each forecast lead time. On the other hand, the cases with the initial MWS error above -10 m s^{-1} (smaller errors) had better TC track simulation performance than the prior cases. The more the initial intensity was underestimated, the worse the TC track simulation performance was. We further performed additional TC simulations to improve the underestimated initial TC intensity by applying the DI scheme. Compared to the CTL runs, the DI runs were similar in TC intensity to the RSMC best track, although the TCs of CTL runs and DI runs were located in similar positions at the initial time. Analyzing the simulated TC track, the performance of the TC track simulations of the DI runs was better than that of the CTL runs, with an improvement of approximately 20.3 % for TPE at 72-h.

The PVT framework was applied to understand the influence of the initial TC intensity on TC motion. To focus on the impact of the initial TC intensity, we analyzed the TC motion at the early stages of the simulations. It was possible to diagnose the simulated TC motion similarly through the PVT framework for both CTL runs and DI runs. Based on the diagnosed TC motion, the dominant components for the TC motion among HA, VA, and DH in the PVT equation were investigated. The dominant components were identified by their magnitude and direction compared to the motion vector calculated by the PVT framework. In the CTL runs, HA aligned in a direction similar to the direction of the diagnosed TC motion vector, while VA contributed to the direction opposite to the diagnosed TC motion vector. Consequently, HA was the dominant term in the CTL runs, with VA and DH having smaller contributions to the simulated TC motion. Analyzing the vectors of the diagnosed TC motion in the DI runs, both HA and VA aligned in the direction of TC motion in most cases. In particular, the impact of VA on the TC motion in the DI runs could be much more significant than that in the CTL runs. To analyze the differences in VA representing the impact of the TC structure, we compared the azimuthal mean vertical velocity, tangential wind, radial wind, and temperature anomaly for the CTL and DI runs. Compared to that of the CTL run, the TC structure of the DI run was well developed through the DI scheme. In the DI runs, a stronger updraft was around the simulated TC center than in the CTL runs. In addition, the simulated TCs in the DI runs had a higher height and larger size compared to the TCs in the CTL runs. With these features, there was stronger convergence in the lower layers and divergence in the upper layers for the simulated TCs in the DI runs. Furthermore, a large vertical gradient of potential vorticity and strong vertical motion was found around the TC center in the DI runs. These were conditions that led to a much greater impact of vertical advection in PVT diagnosis to TC motion in the DI run than in the CTL runs. The well vertically developed TC circulation, which could strongly influence VA, was identified in the DI runs in comparison to that in the CTL run.

In this study, we found that the initial TC intensity error affects the performance of the TC track simulations. We showed that the improvement in the initial intensity led to improved performance in simulating TC tracks. In addition, the impact of the vertical structure with the horizontal asymmetric flow was meaningful in the TC motion. In addition to the influences of horizontal and vertical advections on TC motion, diabatic heating can also play some role in TC motion (Choi et al., 2013; Hsu et al., 2021). A balanced analysis of HA, VA, and DH is required to understand TC motion fully when analyzing the TC motion through the PVT framework. Also, the PVT framework provides insight into the inherent motion of the TC itself. However, it is essential to recognize that the motion of a TC is influenced not only by its dynamics but also by interactions with its surrounding environment (Liu and Xie, 2012; Song et al., 2013; Wang et al., 2019; Lander, 1996). The DI scheme contributed to improvement in TC track simulation for 60-72 h. However, the PVT and TC structures were similar between the CTL runs and the DI runs (Supplementary Fig. S2 and S3). Explaining the improvements in TC dynamics during the later stages of the simulation remains challenging. Considering both the TC and surrounding environmental factors concurrently is crucial for a comprehensive understanding of TC motion. Note that the HA in PVT diagnostics includes both internal and external influences of the flow field. In addition, although the contribution of diabatic heating to the diagnosed TC motion in the simulations discussed in this study is relatively weak, it should be further examined as indicated by previous studies (e.g., see a review by Elsberry et al., 2013). It is also clear that TCs are significantly influenced by interannual and seasonal variability. As a further study, it would be valuable to analyze the impact of initial intensity error on simulated TC track over time periods such as a season or of the El Niño-Southern Oscillation (ENSO).

CRediT authorship contribution statement

Kyoungmin Kim: Writing – original draft, Validation, Methodology, Investigation, Formal analysis, Conceptualization. **Woojin Cho:** Methodology, Conceptualization. **Dong-Hyun Cha:** Writing – review & editing, Supervision, Project administration, Methodology, Funding acquisition, Conceptualization. **Jinyoung Park:** Writing – review & editing, Methodology. **Yuqing Wang:** Writing – review & editing, Methodology. **Johnny C.L. Chan:** Writing – review & editing, Methodology.

Declaration of competing interest

The authors declare that they have no known competing financial interests or personal relationships that could have appeared to influence the work reported in this paper.

Acknowledgments

This work was funded by the Korea Meteorological Administration Research and Development Program under Grant KMI (RS-2023-00241809).

Appendix A. Dynamical initialization

The dynamical initialization (DI) scheme of Cha and Wang (2013) consists of four steps: (1) model integration, (2) vortex separation, (3) performing cycle runs for the tropical cyclone (TC) vortex spin-up, and (4) relocation. First, a 6-h model integration was conducted from the initial time t_0-6 h, which corresponds to 6-h before the initial time t_0. The DI scheme aims to enhance only the vortex field of TC while preserving the environmental factors as much as possible. To enhance the vortex field of the TC, the filtering technique proposed by Kurihara et al. (1993) was used to separate the t_0 simulate field and the t_0-6 h initial field into the vortex and environmental fields. The TC vortex field was defined as

$$F_V = F - F_E$$

where F_V was the vortex field, F was the total field, and F_E was the environmental field. Furthermore, the vortex field was divided into axisymmetric and asymmetric vortex fields with the following cylindrical filter as

$$F_V = F_V^{as} + F_V^{ax}$$

where F_V^{as} was the asymmetric component and F_V^{ax} was the axisymmetric vortex defined as

$$F_v^{ax}(r) = \frac{1}{2\pi}\oint F_V(r,\theta)d\theta$$

The axisymmetric vortex of the t_0 simulated field was weighted according to the TC radius, as described by Cha and Wang (2013), and then combined with the t_0−6 h initial field. The updated t_0−6 h initial field was used to perform a 6-h model integration. The updated t_0−6 h initial field was defined as

$$F^N(x,y,z,t_0-6) = F_E(x,y,z,t_0-6) + F_V^{as}(x,y,z,t_0-6) + \omega F_V^{ax}(x,y,z,t_0-6) + (1-\omega)F_V^{ax,N-1}(x,y,z,t_0)$$

where $F^N(x,y,z,t_0-6)$ was the total field in the Nth cycle run at t_0−6 h, $F_E(x,y,z,t_0-6)$ was the environmental field at t_0−6 h, $F_V^{as}(x,y,z,t_0-6)$ was the asymmetric vortex at t_0−6 h, $F_V^{ax}(x,y,z,t_0-6)$ was the axisymmetric vortex as t_0−6 h, and $F_V^{ax,N-1}(x,y,z,t_0)$ was the axisymmetric vortex in the N − 1 th cycle run at t_0.

This process was repeated until the absolute difference between the TC intensity in the best track and the simulated intensity was less than 10 % of the best track TC intensity. At least two cycle runs were performed. Additionally, spectral nudging (von Storch et al., 2000) was applied during all cycle runs to minimize deviations from the large-scale environmental field:

$$\frac{\partial Q}{\partial t} = F(Q) + \alpha\left(Q_G^L - Q_R^L\right)$$

where Q is the model prognostic variable, F is the model operator, α is a nudging coefficient, Q_G^L and Q_R^L are the large-scale components of the global analysis and WRF model simulation, respectively. The nudging coefficient was set to 0.0003 s^{-1} corresponding to an e-folding damping time of 55.6 min. The spectral nudging was applied to the large-scale component of the wind field above the planetary boundary layer, with wavelengths larger than 1000 km.

Appendix B. Supplementary data

Supplementary data to this article can be found online at https://doi.org/10.1016/j.atmosres.2024.107865.

Data availability

The National Centers for Environmental Prediction (NCEP) final (FNL) Operational Global analysis data on 1° × 1° grids are obtained from https://rda.ucar.edu/datasets/ds083.2/. The Regional Sepcialized Meteorological Centers (RSMC) best track data are obtained from https://www.jma.go.jp/jma/jma-eng/jma-center/rsmc-hp-pub-eg/besttrack.html.

References

Ashcroft, J., Schwendike, J., Griffiths, S.D., Ross, A.N., Short, C.J., 2021. The impact of weak environmental steering flow on tropical cyclone track predictability. Q. J. R. Meteorol. Soc. 147 (741), 4122–4142. https://doi.org/10.1002/qj.4171.

Cao, Y., Fovell, R.G., Corbosiero, K.L., 2011. Tropical cyclone track and structure sensitivity to initialization in idealized simulations: A preliminary study. Terr. Atmos. Ocean. Sci. 22 (6), 559.

Cha, D.-H., Wang, Y., 2013. A Dynamical Initialization Scheme for Real-Time Forecasts of Tropical Cyclones Using the WRF Model. Mon. Weather Rev. 141 (3), 964–986. https://doi.org/10.1175/MWR-D-12-00077.1.

Chan, J.C.L., 1985. Identification of the Steering Flow for Tropical Cyclone Motion from Objectively Analyzed Wind Fields. Mon. Weather Rev. 113 (1), 106–116. https://doi.org/10.1175/1520-0493(1985)113<0106:IOTSFF>2.0.CO;2.

Chan, J.C.L., Gray, W.M., 1982. Tropical Cyclone Movement and Surrounding Flow Relationships. Mon. Weather Rev. 110 (10), 1354–1374. https://doi.org/10.1175/1520-0493(1982)110<1354:TCMASF>2.0.CO;2.

Chan, J.C.L., Ko, F.M.F., Lei, Y.M., 2002. Relationship between Potential Vorticity Tendency and Tropical Cyclone Motion. J. Atmos. Sci. 59 (8), 1317–1336. https://doi.org/10.1175/1520-0469(2002)059<1317:RBPVTA>2.0.CO;2.

Chen, G., Zhang, X., Yang, M., Yu, H., Cao, Q., 2021. Performance of tropical cyclone forecasts in the western North Pacific in 2017. Trop. Cyclone Res. Rev. 10 (1), 1–15. https://doi.org/10.1016/j.tcrr.2021.03.002.

Cho, W., Park, J., Moon, J., Cha, D.-H., Moon, Y.-M., Kim, H.-S., Noh, K.-J., Park, S.-H., 2022. Effects of topography and sea surface temperature anomalies on heavy rainfall induced by Typhoon Chaba in 2016. Geosci. Lett. 9 (1), 29. https://doi.org/10.1186/s40562-022-00230-1.

Choi, Y., Yun, K.-S., Ha, K.-J., Kim, K.-Y., Yoon, S.-J., Chan, J.C.L., 2013. Effects of Asymmetric SST Distribution on Straight-Moving Typhoon Ewiniar (2006) and Recurving Typhoon Maemi (2003). Mon. Weather Rev. 141 (11), 3950–3967. https://doi.org/10.1175/MWR-D-12-00207.1.

Choi, Y., Cha, D.-H., Lee, M.-I., Kim, J., Jin, C.-S., Park, S.-H., Joh, M.-S., 2017. Satellite radiance data assimilation for binary tropical cyclone cases over the western North Pacific. J. Adv. Model. Earth Syst. 9 (2), 832–853. https://doi.org/10.1002/2016MS000826.

Dudhia, J., 1989. Numerical Study of Convection Observed during the Winter Monsoon Experiment Using a Mesoscale Two-Dimensional Model. J. Atmos. Sci. 46 (20), 3077–3107. https://doi.org/10.1175/1520-0469(1989)046<3077:Nsocod>2.0.Co;2.

Elsberry, L.E., Chen, L.-S., Davidson, J., Rogers, R., Wang, Y., Wu, L., 2013. Advances in understanding and forecasting rapidly changing phenomena in tropical cyclones. Trop. Cyclone Res. Rev. 2, 13–24. https://doi.org/10.6057/2013TCRR01.02.

Fiorino, M., Elsberry, R.L., 1989. Contributions to Tropical Cyclone Motion by Small, Medium and Large Scales in the Initial Vortex. Mon. Weather Rev. 117 (4), 721–727. https://doi.org/10.1175/1520-0493(1989)117<0721:CTTCMB>2.0.CO;2.

Gentry, M.S., Lackmann, G.M., 2010. Sensitivity of Simulated Tropical Cyclone Structure and Intensity to Horizontal Resolution. Mon. Weather Rev. 138 (3), 688–704. https://doi.org/10.1175/2009MWR2976.1.

George, J.E., Gray, W.M., 1976. Tropical Cyclone Motion and Surrounding Parameter Relationships. J. Appl. Meteoro. (1962-1982) 15 (12), 1252–1264. http://www.jstor.org/stable/26177612.

Hodges, K.I., Klingaman, N.P., 2019. Prediction Errors of Tropical Cyclones in the Western North Pacific in the Met Office Global Forecast Model. Weather Forecast. 34 (5), 1189–1209. https://doi.org/10.1175/WAF-D-19-0005.1.

Hong, S.-Y., Lim, J.-O.J., 2006. The WRF single-moment 6-class microphysics scheme (WSM6). Asia-Pac. J. Atmos. Sci. 42 (2), 129–151.

Hong, S.-Y., Noh, Y., Dudhia, J., 2006. A New Vertical Diffusion Package with an Explicit Treatment of Entrainment Processes. Mon. Weather Rev. 134 (9), 2318–2341. https://doi.org/10.1175/MWR3199.1.

Hsiao, L.-F., Liou, C.-S., Yeh, T.-C., Guo, Y.-R., Chen, D.-S., Huang, K.-N., Terng, C.-T., Chen, J.-H., 2010. A Vortex Relocation Scheme for Tropical Cyclone Initialization in Advanced Research WRF. Mon. Weather Rev. 138 (8), 3298–3315. https://doi.org/10.1175/2010MWR3275.1.

Hsu, L.-H., Su, S.-H., Kuo, H.-C., 2021. A Numerical Study of the Sensitivity of Typhoon Track and Convection Structure to Cloud Microphysics. J. Geophys. Res.-Atmos. 126 (17), e2020JD034390. https://doi.org/10.1029/2020JD034390.

Kain, J.S., 2004. The Kain–Fritsch Convective Parameterization: An Update. J. Appl. Meteorol. 43 (1), 170–181. https://doi.org/10.1175/1520-0450(2004)043<0170:TKCPAU>2.0.CO;2.

Kurihara, Y., Bender, M.A., Ross, R.J., 1993. An Initialization Scheme of Hurricane Models by Vortex Specification. Mon. Weather Rev. 121 (7), 2030–2045. https://doi.org/10.1175/1520-0493(1993)121<2030:AISOHM>2.0.CO;2.

Kwon, I.-H., Cheong, H.-B., 2010. Tropical Cyclone Initialization with a Spherical High-Order Filter and an Idealized Three-Dimensional Bogus Vortex. Mon. Weather Rev. 138 (4), 1344–1367. https://doi.org/10.1175/2009MWR2943.1.

Lander, M.A., 1996. Specific Tropical Cyclone Track Types and Unusual Tropical Cyclone Motions Associated with a Reverse-Oriented Monsoon Trough in the Western North Pacific. Weather and Forecasting 11 (2), 170–186. https://doi.org/10.1175/1520-0434(1996)011<0170:STCTTA>2.0.CO;2.

Liu, B., Xie, L., 2012. A Scale-Selective Data Assimilation Approach to Improving Tropical Cyclone Track and Intensity Forecasts in a Limited-Area Model: A Case Study of Hurricane Felix (2007). Weather and. Forecasting 27 (1), 124–140. https://doi.org/10.1175/WAF-D-10-05033.1.

Liu, H.-Y., Tan, Z.-M., 2016. A Dynamical Initialization Scheme for Binary Tropical Cyclones. Mon. Weather Rev. 144 (12), 4787–4803. https://doi.org/10.1175/MWR-D-16-0176.1.

Liu, H.-Y., Wang, Y., Xu, J., Duan, Y., 2018. A Dynamical Initialization Scheme for Tropical Cyclones under the Influence of Terrain. Weather Forecast. 33 (3), 641–659. https://doi.org/10.1175/WAF-D-17-0139.1.

Lorenz, E.N., 1963. Deterministic Nonperiodic Flow. J. Atmos. Sci. 20 (2), 130–141. https://doi.org/10.1175/1520-0469(1963)020<0130:DNF>2.0.CO;2.

Lui, Y.S., Tse, L.K.S., Tam, C.-Y., Lau, K.H., Chen, J., 2021. Performance of MPAS-A and WRF in predicting and simulating western North Pacific tropical cyclone tracks and intensities. Theor. Appl. Climatol. 143 (1), 505–520. https://doi.org/10.1007/s00704-020-03444-5.

Ma, Z., Fei, J., Huang, X., Cheng, X., 2012. Sensitivity of tropical cyclone intensity and structure to vertical resolution in WRF. Asia-Pac. J. Atmos. Sci. 48 (1), 67–81. https://doi.org/10.1007/s13143-012-0007-5.

Majumdar, S.J., Magnusson, L., Bechtold, P., Bidlot, J.R., Doyle, J.D., 2023. Advanced Tropical Cyclone Prediction Using the Experimental Global ECMWF and Operational Regional COAMPS-TC Systems. Mon. Weather Rev. 151 (8), 2029–2048. https://doi.org/10.1175/MWR-D-22-0236.1.

Miyachi, T., Enomoto, T., 2021. Tropical Cyclone Track Forecasts Using NCEP-GFS with Initial Conditions from Three Analyses. SOLA 17, 140–144. https://doi.org/10.2151/sola.2021-025.

Mlawer, E.J., Taubman, S.J., Brown, P.D., Iacono, M.J., Clough, S.A., 1997. Radiative transfer for inhomogeneous atmospheres: RRTM, a validated correlated-k model for the longwave. J. Geophys. Res.-Atmos. 102 (D14), 16663–16682. https://doi.org/10.1029/97JD00237.

Mohan, P.R., Srinivas, C.V., Yesubabu, V., Baskaran, R., Venkatraman, B., 2019. Tropical cyclone simulations over Bay of Bengal with ARW model: Sensitivity to cloud microphysics schemes. Atmos. Res. 230, 104651. https://doi.org/10.1016/j.atmosres.2019.104651.

Mohanty, U.C., Osuri, K.K., Routray, A., Mohapatra, M., Pattanayak, S., 2010. Simulation of Bay of Bengal Tropical Cyclones with WRF Model: Impact of Initial and Boundary Conditions. Mar. Geod. 33 (4), 294–314. https://doi.org/10.1080/01490419.2010.518061.

Moon, M., Ha, K.-J., 2019. Effect of typhoon-generated cold wake on the subsequent Typhoon Tembin and its sensitivity to horizontal resolutions. Atmosphere 10 (11), 644.

Moon, J., Park, J., Cha, D.-H., 2021a. Does Increasing Model Resolution Improve the Real-Time Forecasts of Western North Pacific Tropical Cyclones? Atmosphere 12 (6), 776 https://www.mdpi.com/2073-4433/12/6/776.

Moon, J., Park, J., Cha, D.-H., Moon, Y., 2021b. Five-Day Track Forecast Skills of WRF Model for the Western North Pacific Tropical Cyclones. Weather Forecast. 36 (4), 1491–1503. https://doi.org/10.1175/WAF-D-20-0092.1.

Neumann, C.J., Pelissier, J.M., 1981. Models for the Prediction of Tropical Cyclone Motion over the North Atlantic: An Operational Evaluation. Mon. Weather Rev. 109 (3), 522–538. https://doi.org/10.1175/1520-0493(1981)109<0522:MFTPOT>2.0.CO;2.

Park, J., Moon, J., Cho, W., Cha, D.-H., Lee, M.-I., Chang, E.-C., Kim, J., Park, S.-H., An, J., 2023. Sensitivity of Real-Time Forecast for Typhoons Around Korea to Cumulus and Cloud Microphysics Schemes. J. Geophys. Res.-Atmos. 128 (3), e2022JD036709. https://doi.org/10.1029/2022JD036709.

Powell, M.D., Aberson, S.D., 2001. Accuracy of United States Tropical Cyclone Landfall Forecasts in the Atlantic Basin (1976–2000). Bull. Am. Meterol. Soc. 82 (12), 2749–2768. https://doi.org/10.1175/1520-0477(2001)082<2749:AOUSTC>2.3.CO;2.

Schwartz, C.S., Liu, Z., Huang, X.-Y., Kuo, Y.-H., Fong, C.-T., 2013. Comparing Limited-Area 3DVAR and Hybrid Variational-Ensemble Data Assimilation Methods for Typhoon Track Forecasts: Sensitivity to Outer Loops and Vortex Relocation. Mon. Weather Rev. 141 (12), 4350–4372. https://doi.org/10.1175/MWR-D-13-00028.1.

Skamarock, W.C., Klemp, J.B., Dudhia, J., Gill, D.O., Barker, D.M., Duda, M.G., Huang, X.-Y., Wang, W., Powers, J.G., 2008. A description of the advanced research WRF version 3. NCAR Techn. Note 475, 113.

Song, J., Wu, R., Quan, W., Yang, C., 2013. Impact of the subtropical high on the extratropical transition of tropical cyclones over the western North Pacific. Acta Meteorol. Sin. 27 (4), 476–485. https://doi.org/10.1007/s13351-013-0410-6.

Thu, T.V., Krishnamurti, T.N., 1992. Vortex initialization for typhoon track prediction. Meteorog. Atmos. Phys. 47 (2), 117–126. https://doi.org/10.1007/BF01025612.

Torn, R.D., Elless, T.J., Papin, P.P., Davis, C.A., 2018. Tropical Cyclone Track Sensitivity in Deformation Steering Flow. Mon. Weather Rev. 146 (10), 3183–3201. https://doi.org/10.1175/MWR-D-18-0153.1.

von Storch, H., Langenberg, H., Feser, F., 2000. A Spectral Nudging Technique for Dynamical Downscaling Purposes. Mon. Weather Rev. 128 (10), 3664–3673. https://doi.org/10.1175/1520-0493(2000)128<3664:ASNTFD>2.0.CO;2.

Wang, Y., 1998. On the bogusing of tropical cyclones in numerical models: The influence of vertical structure. Meteorog. Atmos. Phys. 65, 153–170.

Wang, Y., & Holland, G. J. (1996). Tropical Cyclone Motion and Evolution in Vertical Shear. J. Atmos. Sci., 53(22), 3313-3332. doi:10.1175/1520-0469(1996)053<3313:TCMAEI>2.0.CO;2.

Wang, D., Liang, X., Zhao, Y., Wang, B., 2008. A Comparison of Two Tropical Cyclone Bogussing Schemes. Weather Forecast. 23 (1), 194–204. https://doi.org/10.1175/2007WAF2006094.1.

Wang, Y., Sun, Y., Liao, Q., Zhong, Z., Hu, Y., Liu, K., 2017. Impact of initial storm intensity and size on the simulation of tropical cyclone track and western Pacific subtropical high extent. J. Meteorol. Res. 31 (5), 946–954. https://doi.org/10.1007/s13351-017-7024-3.

Wang, T., Zhong, Z., Sun, Y., Wang, J., 2019. Impacts of tropical cyclones on the meridional movement of the western Pacific subtropical high. Atmos. Sci. Lett. 20 (5), e893. https://doi.org/10.1002/asl.893.

Wu, L., Chen, X., 2016. Revisiting the steering principal of tropical cyclone motion in a numerical experiment. Atmos. Chem. Phys. 16 (23), 14925–14936. https://doi.org/10.5194/acp-16-14925-2016.

Wu, L., Wang, B., 2000. A Potential Vorticity Tendency Diagnostic Approach for Tropical Cyclone Motion. Mon. Weather Rev. 128 (6), 1899–1911. https://doi.org/10.1175/1520-0493(2000)128<1899:APVTDA>2.0.CO;2.

Xiao, Q., Chen, L., Zhang, X., 2009. Evaluations of BDA Scheme Using the Advanced Research WRF (ARW) Model. J. Appl. Meteorol. Climatol. 48 (3), 680–689. https://doi.org/10.1175/2008JAMC1994.1.

Xie, T., Wu, L., Yu, J., 2022. Application of potential vorticity tendency diagnosis method to high-resolution simulation of tropical cyclones [Original Research]. Front. Earth Sci. 10. https://doi.org/10.3389/feart.2022.994647.

Yamada, H., Nasuno, T., Yanase, W., Satoh, M., 2016. Role of the Vertical Structure of a Simulated Tropical Cyclone in Its Motion: A Case Study of Typhoon Fengshen (2008). SOLA 12, 203–208. https://doi.org/10.2151/sola.2016-041.

Yamaguchi, M., Nakazawa, T., Aonashi, K., 2012. Tropical cyclone track forecasts using JMA model with ECMWF and JMA initial conditions. Geophys. Res. Lett. 39 (9). https://doi.org/10.1029/2012GL051473.

Zhang, S., Pu, Z., 2019. Numerical Simulation of Rapid Weakening of Hurricane Joaquin with Assimilation of High-Definition Sounding System Dropsondes during the Tropical Cyclone Intensity Experiment: Comparison of Three- and Four-Dimensional Ensemble–Variational Data Assimilation. Weather Forecast. 34 (3), 521–538. https://doi.org/10.1175/WAF-D-18-0151.1.

Zhang, C., Wang, Y., 2018. Why is the simulated climatology of tropical cyclones so sensitive to the choice of cumulus parameterization scheme in the WRF model? Clim. Dyn. 51 (9), 3613–3633. https://doi.org/10.1007/s00382-018-4099-1.

Zhang, X., Xiao, Q., Fitzpatrick, P.J., 2007. The Impact of Multisatellite Data on the Initialization and Simulation of Hurricane Lili's (2002) Rapid Weakening Phase. Mon. Weather Rev. 135 (2), 526–548. https://doi.org/10.1175/MWR3287.1.

Zhao, X., Chan, J.C.L., 2017. Changes in tropical cyclone intensity with translation speed and mixed-layer depth: idealized WRF-ROMS coupled model simulations. Q. J. R. Meteorol. Soc. 143 (702), 152–163. https://doi.org/10.1002/qj.2905.